A Learning Scheme for EMG Based Decoding of Dexterous, In-Hand Manipulation Motions

Anany Dwivedi, Yongje Kwon, Andrew J. McDaid, and Minas Liarokapis

***Abstract*— Electromyography (EMG) based interfaces are the most common solutions for the control of robotic, orthotic, prosthetic, assistive, and rehabilitation devices, translating myoelectric activations into meaningful actions. Over the last years, a lot of emphasis has been put into the EMG based decoding of human intention, but very few studies have been carried out focusing on the continuous decoding of human motion. In this work, we present a learning scheme for the EMG based decoding of object motions in dexterous, in-hand manipulation tasks. We also study the contribution of different muscles while performing these tasks and the effect of the gender and hand size in the overall decoding accuracy. To do that, we use EMG signals derived from 16 muscle sites (8 on the hand and 8 on the forearm) from 11 different subjects and an optical motion capture system that records the object motion. The object motion decoding is formulated as a regression problem using the Random Forests methodology. Regarding feature selection, we use the following time-domain features: root mean square, waveform length and zero crossings. A 10-fold cross validation procedure is used for model assessment purposes and the feature variable importance values are calculated for each feature. This study shows that subject specific, hand specific, and object specific decoding models offer better decoding accuracy that the generic models.**

***Index Terms*— Electromyography, human-robot interaction, learning systems, machine learning, prosthetics.**

I. Introduction

ROBOTIC devices are increasingly being used in everyday life tasks (e.g., service robotics, robotic teleoperation and telemanipulation, and clinical applications). However, new human machine interfaces are needed that will allow users to operate such devices in an intuitive manner. Simplistic interfaces like joysticks and mechanical buttons have been used, but such devices require a steep learning curve for the user to control the robot efficiently and offer limited functionality. An alternative would be to control such devices using Electromyography (EMG) based interfaces that offer an intuitive operation [1]. EMG based interfaces rely on the decoding of human motion from the myoelectric activations of the human muscles and they have been used for teleoperation of robotic arm-hand systems [2], [3], rehabilitation using robotic exoskeletons [4], entertainment (myo-games) [5], and for developing muscle computer interfaces [6].

Past studies have focused on sEMG based control of reach to grasp motions [3], execution of various types of grasps [7] and finger movements [8], [9]. But still, complex tasks such as in-hand manipulation of an object or decoding of continuous human-hand motion to control a robot hand in dexterous manipulation tasks, are relatively unexplored. In Equilibrium Point Manipulation (EPM), the finger contact points remain relatively stationary (involve only some infinitesimal, local rolling and slipping) on the object surface, while the object is manipulated. A few applications of such type of motion could be for object inspection or for in-hand object reorientation, by a user teleoperating a robotic arm-hand system or by an amputee controlling a prosthesis. Researchers have focused on the design and development of robot hands capable to achieve EPM [10], but development of an EMG based control scheme that facilitates the execution of EPM tasks with a robotic/prosthetic hand is yet to be achieved.

It must also be noted that each subject is different in the way they utilize their muscles to perform the same in-hand manipulation tasks [11], [12]. In [12], the authors demonstrate that different subjects use different muscle synergies for the same tasks. They attribute these differences in muscle synergies to different hand sizes, kinematics, and musculotendon sizes across the subjects. In [13], the authors discuss the variations in the flexion-extension joint centers of the fingers as well as the segment lengths as a result of of different hand lengths which may cause difference in the kinematics of the hand. Furthermore, in [14], the authors discuss that the different thicknesses of the skin and muscles affect the myoelectric activations in different ways, generating complex EMG signals that are subject specific. These findings motivated us to focus on the development of a learning scheme that gerenerates subject, object, and hand specific models for decoding the object motion during the execution of dexterous, in-hand manipulation tasks.

In our previous work, we proposed a preliminary learning scheme based on the Random Forests regression method that maps the myoelectric activations of the muscles of the forearm and the hand to the motion of the object [15] and we studied the optimal muscle selection for the sEMG based decoding of these in-hand manipulation motions [11]. In this study,

Manuscript received January 30, 2019; revised July 2, 2019; accepted August 9, 2019. Date of publication August 21, 2019; date of current version October 8, 2019. *(Corresponding author: Minas Liarokapis.)*

A. Dwivedi, Y. Kwon, and M. Liarokapis are with the New Dexterity Research Group, Department of Mechanical Engineering, The University of Auckland, Auckland 1010, New Zealand (e-mail: minas.liarokapis@auckland.ac.nz).

A. J. McDaid is with the Department of Mechanical Engineering, The University of Auckland, Auckland 1010, New Zealand.

we extend our previous work including experiments with more subjects, objects, and experimental conditions. More precisely, we explore how the EMG signals vary across different subjects of different genders and with different hand sizes, assessing also the decoding models performance.

The rest of the paper is organized as follows: Section II discusses the related work, Section III describes the equipment used, the experimental procedures and the experiments conducted, Section IV reports the methods used to formulate the proposed learning scheme, Section V presents and discusses the results, while Section VI concludes the paper.

II. Related Work

Several researchers have employed EMG based interfaces for executing tasks of everyday life. In [6], Saponas *et al.* proposed a muscle sensing arm-band for finger gesture classification, while in [16], they proposed a human-machine interaction (HMI) scheme, capable of accurately classifying the intention even when the hands are under load. EMG based interfaces have also used in robotic rehabilitation. In [4], authors presented an upper limb exo-skeleton controlled in accordance to the user's intention (decoded using the human myoelectric activations). In [17], Kiguchi *et al.* used EMG and Electroencephalography (EEG) signals for estimating the user's upper limb motions for the control of wearable robots (robotic exo-skeletons). EMG based interfaces can also be used for teleoperation and telemanipulation applications with robot arm hand systems, as they provide an intuitive human-machine interface which allows the user to to control the device with natural arm movements and gestures [18].

In 1938, A.V. Hill proposed a model to simulate the behaviour of the human muscles [19]. But, this model is highly complex and subject specific as it depends on a lot of internal parameters like the muscle fibre length and muscle contraction velocity that vary for different muscle types and subjects. As a result, it becomes a complex and time consuming process to make a model subject and muscle specific. In order to overcome these issues, researchers have focused on machine learning based methods to map the muscular activations to the motions [20], [21]. Generally, a machine learning model based control system for an assistive device using biological signals like sEMG for the model input has mainly three cascaded modules, namely signal pre-processing, feature extraction and classification/regression based output [22].

Before deciding on the required features to be extracted, the raw sEMG signal should be appropriately pre-processed. The first step in pre-processing involves filtering to remove various unwanted noise in the signal. In [23], Balbinot *et al.* used a bandpass filter with 20 Hz as lower cutoff frequency and 500 Hz as higher cutoff frequency to reduce the motion artifacts in the acquired signals. In [24], Zhou *et al.* proposed an adaptive ECG spike clipping algorithm to remove the ECG contamination in the EMG signal. To do this, the Averaged Rectified Value (ARV) of the signal is calculated in a window of length l and a threshold/cutoff level is set as a gain g of the ARV. The signal is clipped and replaced as the cutoff value when it surpasses the threshold value. After filtering the acquired signals, the data is then segmented to compute required feature set. The length of the segment is important as it affects the performance of a classifier or regressor [25]. Studies have found that using a segment length that is smaller than 125 ms leads to high bias and variance in the calculation of features. Where as using a segment length between 125 ms and 500 ms increases the classification accuracy significantly by reducing the bias and variance in the calculated features [26], [27]. But, for prosthetic limb control, the response time should be less than 300 ms in order to reach the real-time constraints [28].

After the signal pre-processing, the next step is to extract appropriate features from the data to improve the performance of the classifier or regressor. This process involves transforming raw bio-signals into a feature vector set. Generally, the extracted features for the analysis of sEMG signals can be divided into three categories, Time Domain (TD), Frequency Domain (FD), and Time-Frequency Domain (TFD) features [29]. The TD features contain the information about the signal that is extracted from the amplitude of the signal, while FD features contain information regarding the Power Spectral Density (PSD) of the signal. TFD features can characterize varying frequency information at different time locations, providing non-stationary information of the analyzed signals. From these three types of features, TD features are most commonly used because: 1) TD features are computationally less expensive to calculate than FD or TFD features and 2) studies which compared TD with FD features reveal that TD features provide a more consistent performance than FD features [27].

Some of the most commonly used TD features for training EMG based intention decoding models are Mean Absolute Value (MAV), Slope Sign Changes (SSC), Zero Crossing (ZC) and Waveform Length (WL) [30]. ZC and SSC provide important information regarding the frequency domain characteristics of the signal, which is computationally expensive to obtain otherwise. According to Hägg [31], ZC is also a measure of fatigue in the muscles. WL is a measure of the complexity of the signal and can also be used as a quantitative measure for the selection of the electrode positions [32]. Computationally, MAV represents the area under the rectified EMG signal and in sense of its physical meaning it quantifies the effort of the examined muscles. Another TD feature that quantifies the effort of the muscles is the Root Mean Square (RMS) value. RMS represents the average power of a signal for a given period of time [33].

Regarding sEMG based decoding of the human intention or motion using Machine Learning, the two most common used approaches are classification and regression. The classification methods give a discrete decision on the user's intention (i.e., identifying the task to be executed), while regression methods result in a continuous decoding of the human motion (i.e., derive specific trajectories). One of the biggest challenges the researchers face while decoding the human motion or intention from the myoelectric activity is the non-linear relationship of the myoelectric signals and the human motion [34]. Due to this, most of the studies have avoided the continuous decoding of human motion and mainly focus on discrete

control of robotic/prosthetic devices e.g., bidirectional control of a robotic wrist [35].

In [36], Castellini *et al.* compared Neural Networks (NN), Support Vector Machines (SVM) and Locally Weighted Projection Regression (LWPR) to classify the type of grasp and decode the grasping forces using the human myoelectric activations. In this work, they concluded that none of the tested approaches clearly outperforms the other, which indicates that the machine learning as a whole is a viable approach. In [37], Adewuyi *et al.* studied the contribution of the intrinsic and the extrinsic muscles of the hand in classification of different types of grasps. In order to do that, they used a Linear Discriminant Analysis (LDA) classifier. They showed that using a combination of intrinsic and extrinsic muscles achieves an accuracy of 96% for partial hand amputees and 100% accuracy for non amputees, while a model trained for extrinsic muscles achieve 73% for partial hand amputees and 88% for non-amputees.

In [38], [39], Liarokapis *et al.* proposed a task-specific framework for myoelectic activations based decoding of the reach to grasp tasks. They compared the performance of RF with LDA, Quadratic Discriminant Analysis (QDA), k-Nearest Neighbours, NN and SVM. For this, they used myoelectric activations of 16 upper and forearm muscles of the human arm and combined the classification and regression techniques in a synergistic manner. From this work they concluded that: i) task-specific models outperform general models trained for the entire problem space and ii) RF methodology based learned models outperform other learning techniques in terms of classification and estimation accuracy.

Several classification methods based on machine learning schemes have been used to identify the user's intention using the activations of muscles of the arm and hand to trigger an appropriate control strategy, like execution of a particular grasp. However, a drawback to this approach is that it uses a set of fixed, predetermined movement strategies. Previous studies that proposed a continuous decoding of the human motion [38], [39] focused only on reach to grasp and grasping motions and not on dexterous manipulation. In this study, we focus on decoding the motion of manipulated object (within the hand) during the execution of dexterous in-hand manipulation tasks, directly from the myoelectric activations of the muscles of human hand and forearm. Such schemes can be used to develop HMI interfaces for immersive user experience that will offer intuitiveness of operation.

III. Apparatus and Experiments

The experiments were performed by 11 able-bodied subjects (age $= 26 \pm 4$, hand length $= 176 \pm 25$), five males (hand length $= 186 \pm 15$) and six females (hand length $= 166 \pm 6$). The study has received the approval of the University of Auckland Human Participants Ethics Committee (UAHPEC) with the reference number #019043. Prior to the study all subjects provided written and informed consent to the experimental procedures. The experiments were performed by each subject with their dominant hand. Three subjects (two males and one female) were left hand dominant while eight subjects (three males and five females) were right hand dominant.

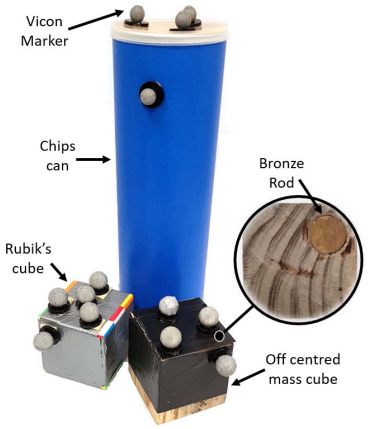

Fig. 1. The objects used for the experiments with the Vicon motion capture system. The objects are: custom made cube with a brass rod in the top corner to off-center the mass of the cube, a Rubik's Cube and a Chips Can. The Rubik's Cube and the Chips Can are from the YCB grasping object set [40]. The Vicon system's motion tracking markers are also depicted.

A. Experimental Setup

The EMG signals were acquired by a g.Tec g.USBamp bioamplifier. A sampling rate of 1200 Hz was used and the signal was bandpass filtered using a Butterworth filter (5 Hz-500 Hz). A notch filter of 50 Hz was applied to reduce the electric noise. To record the motion of the objects while performing the manipulation tasks, a Vicon optical motion capture system that consists of 8 Vicon T-series cameras connected to the Giganet system and appropriate reflective markers was used. The Vicon Tracker software was used to capture the trajectories of the reflective markers. The markers on the objects were placed in a way that they do not affect the natural hand postures during the grasp, as the contact points do not change significantly during EPM. The sampling rate of the Vicon system was 100 Hz. A trigger system was used to facilitate data synchronization of the two data acquisition systems. Due to the differences in sampling rates, the object motion data was upsampled to match the sampling frequency of the EMG data.

B. Experimental Tasks

Each subject was provided with a verbal and visual instruction regarding how the experimental task has to be performed. For the experiment, subjects were asked to perform 3-dimensional equilibrium point manipulation task using the Rubik's cube, and chips can from the Yale-CMU-Berkeley (YCB) grasping object set [40] and a custom made off-centered cube (see Fig. 1). For all the manipulation tasks, each subject was to sit upright with their forearm rested on a custom-made stand. Each manipulation task session was executed with a sequence starting with a 5 sec rest period (where the hand holds the object in a stationary pose), followed by 5 repetitions of the manipulation motion for each trial.

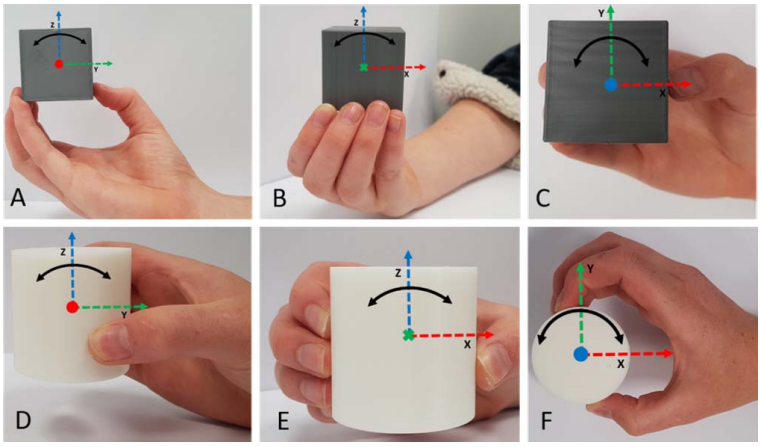

Fig. 2. Instances of manipulation motion performed during the experiment. Subfigure A) shows the Pitch motion for a cube, subfigure B) shows the Roll motion for a cube and subfigure C) shows the Yaw motion for a cube, while subfigure D) shows the Pitch motion for a cylinder, subfigure E) shows the Roll motion for a cylinder and subfigure F) shows the Yaw motion for a cylinder. The axes are color coded and the colored 'Circles' and the 'X' marks at the origins indicate that the axis is orthogonally outward/inward to the page. The thick black colored arrows show the direction of the motion about the out of plane axis.

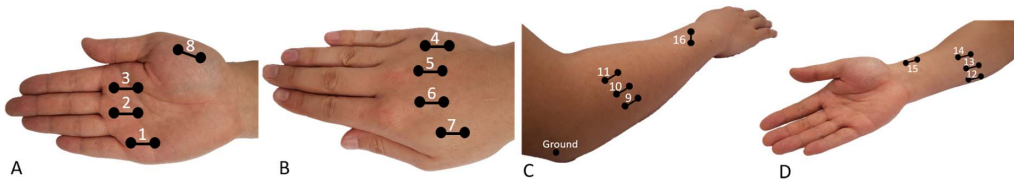

Fig. 3. Electrode placement positions for EMG data collection on the right arm hand system. The double dot with the connected line represents a double-differential EMG electrode. Electrodes 1, 2 and 3 are placed at the front of the palm measuring the Lumbrical muscles' myoelectric activations. Electrodes 4, 5, 6 and 7 are placed at the back of the palm measuring the Interossei muscles' myoelectric activations. Electrode 8 is placed at the base of the thumb measuring the Opponens Pollicis muscle myoelectric activations. Electrodes 9, 10 and 11 measure the myoelectric activations of the Extensor Digitorum muscle site. Electrodes 12, 13 and 14 measure the myoelectric activations of the Flexor Digitorum muscle site. Electrode 15 measures the myoelectric activations of Abductor Pollicis Longus and finally electrode 16 measures the myoelectric activations of Extensor Pollicis Brevis. Ground is represented with a single dot and is placed at the elbow where muscular activity becomes minimal.

TABLE I
NAMES AND LOCATION OF MUSCLES USED IN THIS STUDY

Muscle Name	Lumbrical (x3)	Interossei (x4)	Opponens Pollicis	Extensor Digitorum (x3)	Flexor Digitorum (x3)	Abductor Pollicis Longus	Extensor Pollicis Brevis
Muscle Location	Hand			Forearm			

There were 10 of these trials per session. Adequate resting period was given in between each trial (approximately 30 sec) to reduce the fatigue in the muscles and a rest of approximately 5 min at the end of a session. Fig. 2 visualizes all the manipulation tasks. The different types of manipulation tasks performed during the experiments, are:

- Pitch: a coordinated movement of the fingers that creates a pitch motion of the cube
- Roll: a coordinated movement of the fingers that creates a roll motion of the cube
- Yaw: a coordinated movement of the fingers that creates a yaw motion of the cube

C. Muscle Selection

For all the manipulation tasks, myoelectric activations were measured from 8 muscles of the hand and 8 muscles of the forearm using double differential EMG electrodes (Fig. 3). For the hand, three electrodes were placed on the palm measuring the activity of the Lumbrical muscles, four electrodes were placed at the back of the palm measuring the activity of the Interossei and one electrode was placed on the base of the thumb to measure the myoelectric activations of the Opponens Pollicis muscle. For the forearm, three electrodes were placed on the Extensor Digitorum site, three were placed on the Flexor Digitorum site, one was place on Abductor Pollicis Longus and the final one was placed to measure the myoelectric activations of the Extensor Pollicis Brevis. The Ground electrode was placed on the elbow, where the muscular activity becomes minimal. Table I summarizes the locations of the muscles. The selection of the electrode positions was inspired by existing literature [41], [42] as well as by the Innerbody website [43]. The Innerbody website provides an

accurate 3D muscle anatomy atlas of the human hand and arm, as well as an outline of the contributions of each muscle to the motion of the human joints.

IV. Methodology

A. Feature Extraction

The raw EMG signals were acquired and filtered (5 Hz - 500 Hz Butterworth filter) by the bioamplifier. The signals were segmented using a sliding window of 200 ms with 10 ms increments. Window size and the stride of the window were selected so as to achieve desired performance. It may be noted that the size of the window must not be too large due to real-time constraints. But, the window should be adequately large to avoid high biases and variance [29]. In this work we extract 3 different features from each EMG channel, namely: Root Mean Square Value (RMS) [33], Waveform Length (WL) and Zero Crossings (ZC) [30], [44].

1) Root Mean Square Value: The RMS value is one of the most commonly used values in the TD. It represents the square root of the average power of the signal for the given time period. The RMS value is defined as:

$$RMS = \sqrt{\frac{1}{N}\left(\sum_{k=1}^{N}(x_k)^2\right)}, \tag{1}$$

where N is the size of the window applied to the data.

2) Waveform Length: WL measures the complexity of the signal. It is a measurement of the amplitude of the waveform, frequency, and duration in a single parameter and is defined as:

$$WL = \sum_{k=1}^{N} |\Delta x_k|, \tag{2}$$

where $\Delta x_k = x_k - x_{k-1}$.

3) Zero Crossings: ZC represents the number of times the signal crosses the zero value in a given time period. ZC can be used to estimate the fatigue in the muscles [31]. The count of ZC is incremented when:

$$\begin{gathered} x_k < 0 \quad \&\& \quad x_{k+1} > 0 \\ \| \| \\ x_k > 0 \quad \&\& \quad x_{k+1} < 0 \\ \&\& \\ |x_k - x_{k+1}| > V_t \end{gathered} \tag{3}$$

where V_t is a voltage threshold, which is selected according to the noise in the signal. This algorithm increments ZC only if it falls outside the dead-zone as it tries to eliminate the effect of noise on the zero crossings.

The input dimension of the data for the learning algorithm is 3 EMG features per channel $*$ 16 channels $=$ 48 input features for the model. The output dimension is 1 for each rotation (roll, pitch and yaw) motion of the object.

B. Random Forests Model for Object Motion Decoding

In order to successfully decode the object motion we solve a regression problem that maps the features extracted from the EMG data to the actual motion of the object during in-hand manipulation motion, using the Random Forest (RF) regression methodology. RF is a type of supervised learning algorithm, which was originally proposed by Tin Kam Ho of Bell Labs [45] using the random subspace method. This is a way to implement the "stochastic discrimination" approach to classification proposed by Eugene Kleinberg [46]. An extension to this algorithm was developed by Leo Breiman [47]. His work combines the "Bagging" idea he developed with Ho's idea of feature selection.

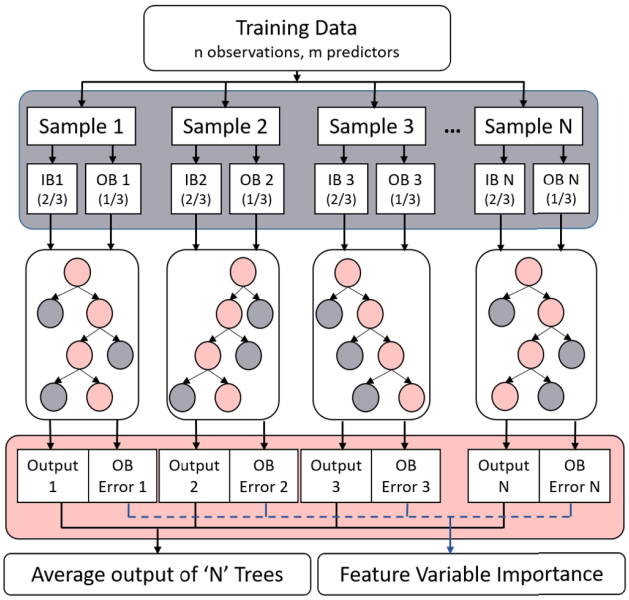

Fig. 4. Flow diagram for the Random Forest based model training. IB N represents N^{th} in-bag training set, OB N represents N^{th} out-of-bag training set and OB Error N represents N^{th} out-of-bag error.

RF is an ensemble of the decision (i.e., it consists of multiple decision trees) trees and can be used for classification and regression. The output of the model is the class with the most number of votes by the trees in the classification case and the average prediction of all the trees in the regression case. Taking an average output from "N" trees regularizes the output, making the predictions less prone to overfitting. A few other advantages of the using RF methodology based prediction models is that these models are very efficient with small and large databases, they do not require huge training dataset, they have fast prediction rate and can efficiently solve multi-dimensional problems. The RF model is created by growing trees using the training set (Fig. 4). This is carried out by randomly selecting the datapoints with replacement. Generally 2/3 (also called as in-bag sample set) of the training set is selected by bagging to train the model. On this set, attribute bagging is performed, which is done to select 'm' features out of total 'M' features of the feature set. Attribute bagging decreases the variance along with the risk of overfitting. For each different value of 'm' a tree is grown and trained using the in-bag sample set. Once the trees are trained they are tested on the remaining 1/3 (also called as out-of-bag sample set) of the training set. The performance of each tree (trained with different feature set) is evaluated and the tree

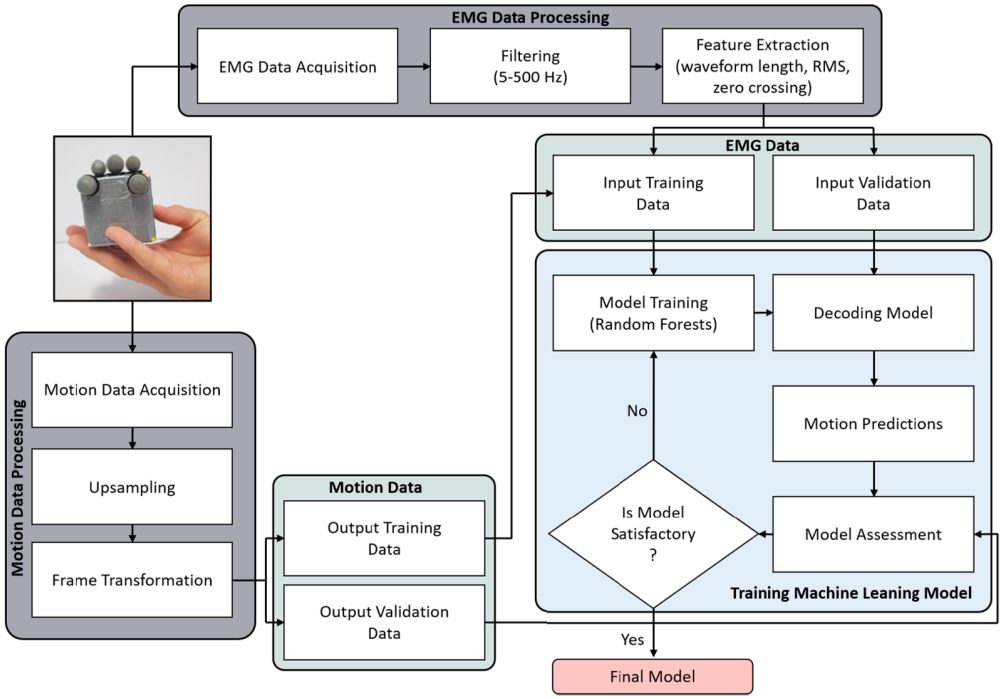

Fig. 5. Block diagram of the proposed EMG-based object motion decoding scheme for in-hand manipulation motions. The EMG signals acquired during the motion were filtered and time domain features were extracted. The object motion data was up sampled and transformed to the object reference frame. This processed data was divided into training and validation set and was used as an input to the RF methodology based learning scheme. The training and validation phases ensure that the predicted data closely follow the true motion data. If the performance of the trained model is not satisfactory, the model is retrained with different RF parameters until the trained model can predict the motion accurately.

with best performance is selected. The error in prediction by each tree is used to evaluate the feature vector importance for minimized error. This process is repeated 'N' times to grow 'N' trees.

C. Learning Framework

In this study, we decode the motion of an object during an in-hand manipulation motion and study how different subjects use different task execution strategies by activating different muscles to perform the same tasks. To do this, we extract the TD features from the EMG data. This is then divided into two sets, one for training and the other for validation. An iterative training and validation was performed to optimize the hyper-parameters (like window size, window stride, RF parameters etc.,). The model with a satisfactory performance was selected as the final model. A detailed flow of the model optimization is described in Fig. 5. The results discussed in Section V are the average of 10-fold cross validation. To compare the performance of the generalized models with the models specific to a subject and an object, we perform analysis in three different sets, namely:

1) Subject-Specific and Object-Specific RF Models: In this set, we develop object specific models for a particular subject.

2) Subject-Specific and Object-Generic RF Models: In this set, we develop object generic models for a particular subject.

3) Subject Generic RF Models: In this set, we group the data collected into females, males, participants with small hand size (hand length <= 165mm), medium hand size (165mm < hand length <= 185mm) and large hand size (hand length > 185mm) and train object specific as well as object generic RF models for each group.

V. Results

In this section, we evaluate the importance of the employed features (muscles) while decoding the manipulation motion on different objects for all the sets discussed in section IV-C. The efficiency of the trained model is assessed by using the Pearson correlation coefficient and the percentage of the NMSE (Normalized Mean Square Error) for accuracy, to compare the predicted and the actual object motion. The NMSE value of 0% implies a bad fit whereas the NMSE value of 100% implies that the two trajectories are identical. The NMSE value is defined as follows:

$$NMSE(\%) = 100 * \quad 1 - \frac{||x_r - x_p||^2}{||x_r - mean(x_r)||^2} \tag{4}$$

where, ||.|| indicates the 2-norm of a vector, x_r is the actual reference motion and x_p refers to the predicted motion.

A. Subject-Specific and Object-Specific RF Models

In this set, subject specific RF models were trained for a particular object. Table II presents the correlation and the accuracy results for decoding the motion. The accuracy of the subject and object specific model is 83%. From the table it can be noted that the subjects with smaller hand sizes have a considerable drop in motion decoding accuracy for the off-center mass cube as compared to the Rubik's cube. Whereas subjects with bigger hand sizes have comparable or better

TABLE II
CORRELATION (C) AND ACCURACY (A) RESULTS FOR SUBJECT AND OBJECT SPECIFIC RF MODEL

Obj.	Rubik's Cube		Chips Can		Off-Center Mass Cube		Hand Size
Subj.	C	A	C	A	C	A	mm
1	92.60	83.61	76.00	52.40	75.67	59.60	165
2	83.62	67.91	76.72	55.68	75.55	55.02	164
3	87.06	74.26	79.77	60.41	86.60	72.15	170
4	61.64	32.49	74.24	49.32	53.45	27.01	163
5	87.86	75.01	77.37	54.95	77.84	56.72	165
6	79.64	57.93	76.15	53.64	83.86	66.65	169
7	89.61	77.91	78.60	59.72	88.49	75.09	170
8	85.78	72.18	83.13	67.35	86.98	73.11	180
9	87.27	73.64	81.44	63.64	85.15	69.38	200
10	78.36	57.88	70.97	45.99	79.30	60.14	190
11	82.89	67.71	78.98	58.61	83.94	68.09	190

performance with the off-center mass cube as compared to the Rubik's cube.

Fig. 6 presents the muscle importances for all the subjects while manipulating each of the objects. It can be observed that all the different subjects utilize different muscle combinations to perform the same motion on the same objects. For the manipulation of the Rubik's cube, Lumbricals were utilzed by subjects 1, 2, 4, 6 and 11. Interossei were utilized by subjects 1, 2, 4, 5, 6, 7, 8, 10 and 11. Opponens Pollicis was used by subjects 1, 2, 4, 5, 9 and 10. Extensor Digitorum muscles were used by subjects 2, 3 and 8. Flexor Digitorum muscles were used by 4, 5, 7 and 8. Abductor Pollicis Longus was utilized by subject 3 and 10 and while only subject 3 utilized Extensor Pollicis Brevis. For the manipulation of the chips can, Lumbricals were utilized by subjects 1, 2, 4 and 6. Interossei were utilized by subjects 2, 3, 10 and 11. Opponens Pollicis was used by subjects 1, 2, 4, 6 and 9. Extensor Digitorum muscles were used by subjects 10 and 11. Flexor Digitorum muscles were used by 7 and 11. Abductor Pollicis Longus was utilized by subject 3, 6, 8 and 9 and Extensor Pollicis Brevis was used by subjects 3, 5 and 7. For the manipulation of the off-centered mass cube, Lumbricals were utilized by subjects 1, 2, 4, 6, 8 and 10. Interossei were utilized by subjects 2, 4, 8, 10 and 11. Opponens Pollicis was used by subjects 1, 2, 3, 4, 5 and 9. Extensor Digitorum muscles were used by subjects 3 and 10. Flexor Digitorum muscles were used by 2, 7 and 8. Abductor Pollicis Longus was utilized by subject 3, 6, 7, 8, 9 and 10 and Extensor Pollicis Brevis was used by subjects 3 and 5. It is evident that most subjects utilize hand muscles more than the muscles of the forearm to perform the in-hand manipulation tasks.

B. Subject-Specific, Object-Generic RF Models

Next we develop subject specific RF models for all objects. Table III, presents the correlation and accuracy for decoding the object motion. It is evident that the subjects with small and large hands have lower object motion decoding accuracy as compared to the subjects with medium hand size. Fig. 7, presents the muscle importance for all the subjects while manipulating each of the objects. From the Fig. 7, it is evident

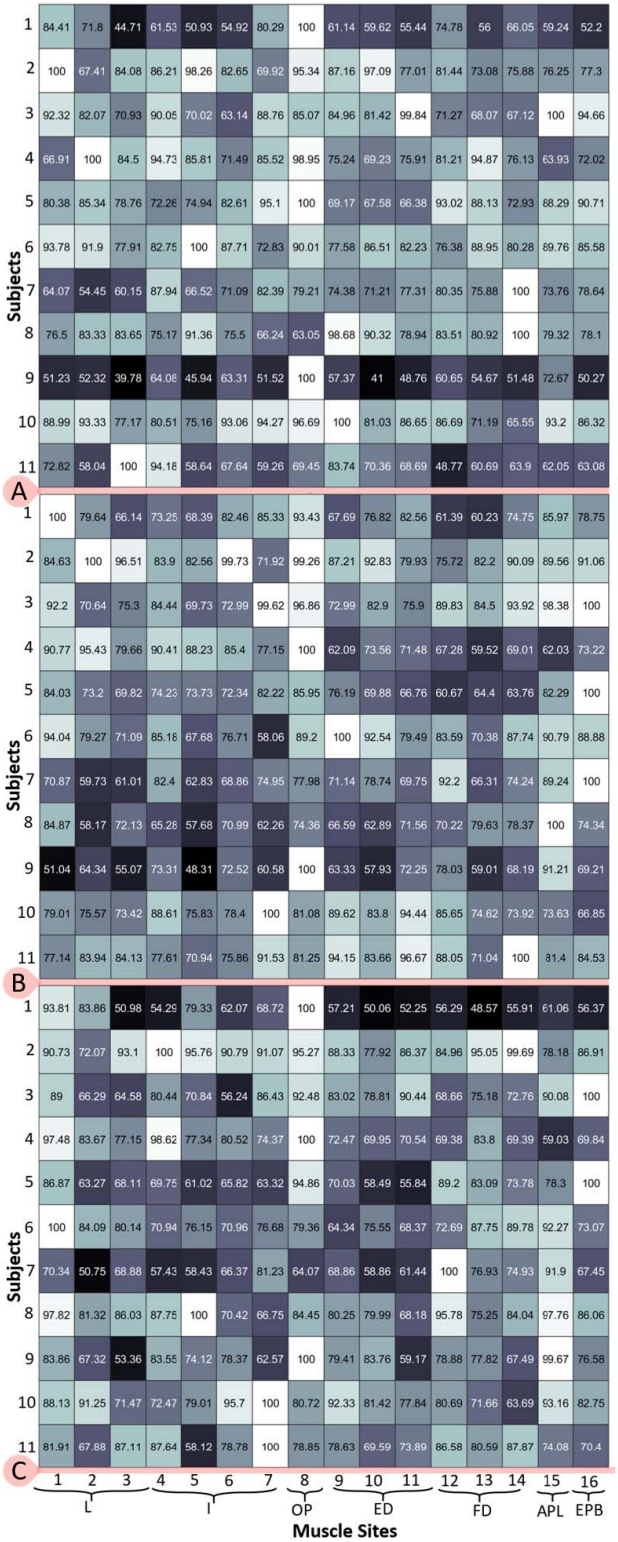

Fig. 6. Comparison of the muscle importance for each subject. Subfigure A) shows muscle importance while manipulating Rubik's cube, subfigure B) shows muscle importance while manipulating the chips can and subfigure C) shows muscle importance while manipulating the off-centered mass cube. Each column represents a muscle observed and each row corresponds to a subject who participated in this study. In x-axis, L represents Lumbricals, I represents Interossei, OP represents Opponens Pollicis, ED represents Extensor Digitorum, FD represents Flexor Digitorum, APL represents Abductor Pollicis Longus, and EPB represents Extensor Pollicis Brevis.

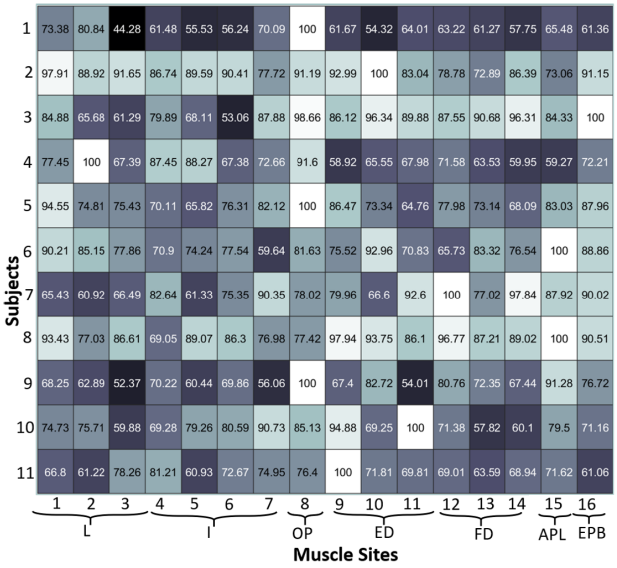

Fig. 7. Comparison of the muscle importance for each subject for object generic RF models. Each column represents a muscle observed and each row corresponds to a subject who participated in this study. In x-axis, L represents Lumbricals, I represents Interossei, OP represents Opponens Pollicis, ED represents Extensor Digitorum, FD represents Flexor Digitorum, APL represents Abductor Pollicis Longus, and EPB represents Extensor Pollicis Brevis.

TABLE III
CORRELATION AND ACCURACY FOR SUBJECT SPECIFIC RF MODELS

Subjects	Correlation (%)	Accuracy (%)	Hand Size (mm)
1	74.37	56.50	165
2	79.00	61.03	164
3	84.24	69.39	170
4	62.70	36.82	163
5	79.96	61.41	165
6	80.14	61.75	169
7	87.05	73.82	170
8	85.76	72.48	180
9	82.41	64.82	200
10	76.16	55.77	190
11	81.29	65.32	190

that to manipulate the 3 objects in 3-dimensional space, different subjects use different muscle groups. Lumbrical muscles were used by subjects 1, 2, 4, 5, 6 and 8. Interossei were used by subjects 2, 7 and 10. Opponens Pollicis was used by subjects 2, 3, 4, 5 and 9. Extensor Digitorum muscle group was used by subjects 2, 3, 6, 7, 8, 10 and 11. Flexor Digitorum muscle group was used by subjects 3, 7 and 8. Abductor Pollicis Longus was used by subjects 6, 8 and 9 and Extensor Pollicis Brevis was used 2, 3, 7 and 8.

C. Subject-Generic RF Models

In this set, we present the results of the correlation and accuracy of the decoded motions along with the importance of the muscles for object specific RF models. Table IV presents the correlation and the accuracy for decoded motions of each of the objects. The group of females (average hand length $\sim 166mm$) and participants with small hand size (hand length <= 165mm) see a drop in motion decoding accuracy. This is similar to the trend observed in Table II.

Fig. 8 shows the muscle importances. It is evident that Opponens Pollicis (muscles of the thumb) is very important

TABLE IV
CORRELATION (C) AND ACCURACY (A) RESULTS FOR THE MODELS TRAINED FOR SPECIFIC SUBJECT GROUPS FOR INDIVIDUAL OBJECT

Objects	Rubik's Cube		Chips Can		Off-Center Mass Cube	
Group	C	A	C	A	C	A
Females	79.87	62.26	75.95	56.07	71.26	52.66
Males	81.86	65.65	76.99	57.06	83.37	67.52
Small Hand	79.76	61.92	75.12	54.09	68.68	49.52
Medium Hand	84.62	70.40	79.99	62.02	85.22	70.80
Large Hand	79.85	62.11	73.93	51.94	80.32	62.31

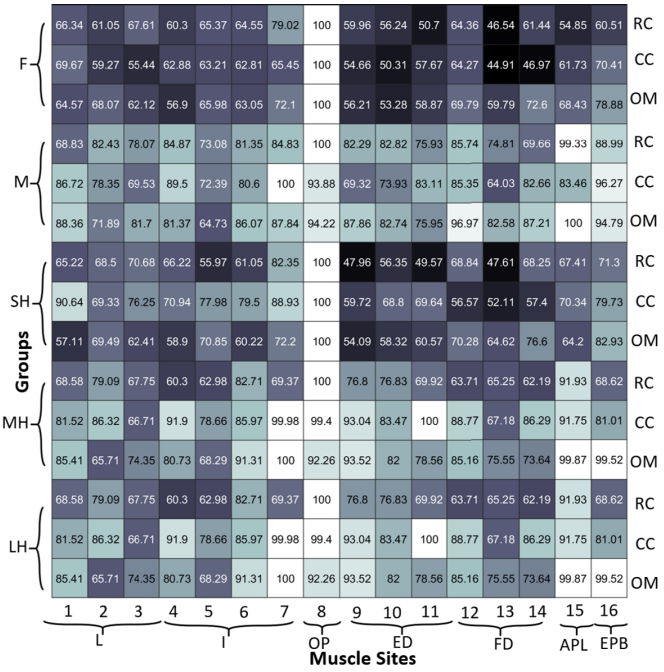

Fig. 8. Comparison of the muscle importance for object specific RF models while manipulating objects in 3-dimensional. In x-axis, L represents Lumbricals, I represents Interossei, OP represents Opponens Pollicis, ED represents Extensor Digitorum, FD represents Flexor Digitorum, APL represents Abductor Pollicis Longus, and EPB represents Extensor Pollicis Brevis. In the y-axis (left), F represents group of female participants, M represents groups of male participants, SH represents participants with small hand size, MH represents participants with medium hand size and LH represents participants with large hand size. In the y-axis (right), RC stands for Rubik's Cube, CC stands for Chips Can and OM stands for Off-center Mass Cube.

TABLE V
CORRELATION AND ACCURACY RESULTS FOR MODELS TRAINED FOR SPECIFIC SUBJECT GROUPS

Groups	Correlation (%)	Accuracy (%)
Females	72.58	51.86
Males	80.70	63.06
Small Hand	70.30	49.31
Medium Hand	83.22	67.58
Large Hand	77.31	57.76

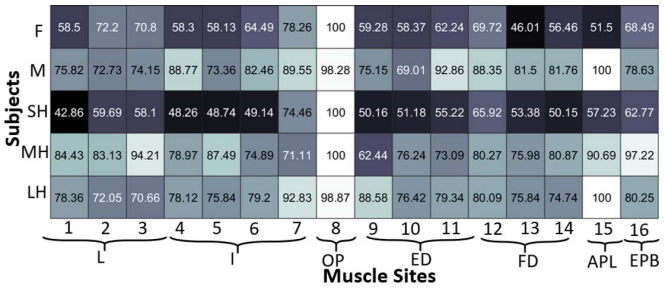

Fig. 9. Comparison of the muscle importance while manipulating objects in 3-dimensional space for all the participant groups. In x-axis, L represents Lumbricals, I represents Interossei, OP represents Opponens Pollicis, ED represents Extensor Digitorum, FD represents Flexor Digitorum, APL represents Abductor Pollicis Longus, and EPB represents Extensor Pollicis Brevis. In the y-axis, F represents group of female partcipants, M represents groups of male participants, SH represents participants with small hand size, MH represents participants with medium hand size and LH represents participants with large hand size.

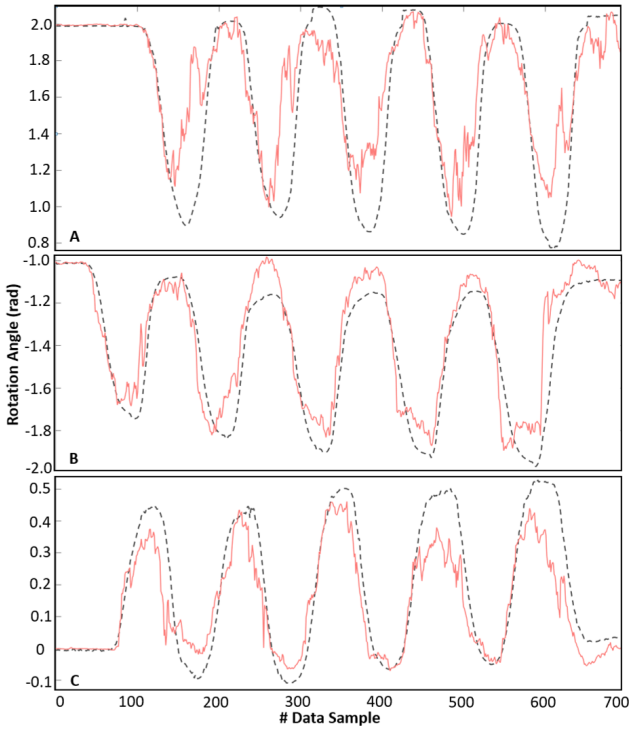

Fig. 10. Plots of actual vs estimated motion from the myoelectric activations of the medium hand size participants. Subfigure A depicts the pitch motion, subfigure B depicts the roll motion and subfigure C depicts the yaw motion. The dashed lines represent the actual motion while the solid lines represent the predicted motion.

while manipulating each of the object. For females (hand length $= 165mm \pm 13$), the importance of the thumb muscles is significantly higher than the other muscles. This trend is also seen in the group of participants with small hand size (hand length $<=$ 165mm). The muscle importances for the group of male participants (e.g., participants with medium and large hand sizes) is not as skewed. A possible explanation for this could be that smaller hand size reduces the manipulation capabilities for an object and thus all the muscles are not properly utilized while performing the motion. Another observation is that the Flexor Digitorum and the Extensor Digitorum for the off-center mass cube have higher importance as compared to the Rubik's cube. The reason could be that these muscles have higher contribution in stabilizing the object due to the off-centered mass.

Finally Table V presents the correlation and the accuracy for the decoded motion for object generic RF models. It can be noticed that the group of participants with medium hand size have the best accuracy of motion decoding while the participants with the small hand size have the lowest accuracy of motion decoding. Fig. 9 shows the importances of the muscles for decoding the object motion. From the figure it is evident that the groups with relatively smaller hand sizes have the highest muscle importance for Opponens Pollicis (the thumb muscle), which is considerably higher than other muscles. While the groups with larger hand sizes have comparatively similar importances of muscles for the hand and the forearm. Fig. 10 shows the actual vs decoded motion for the participants of the medium hand size group.

VI. Discussion and Conclusions

In this work, we have presented an sEMG-based learning scheme for decoding object motion in dexterous, in-hand manipulation tasks and studied the contribution of different muscles towards the decoding of the object motion. To do that, we acquired sEMG signals from specific muscle sites on the human hand and forearm along with the motion data of the object in 3-dimensional space using an optical motion capture system. The analysis was done in 2 parts. In the first part, RF based object specific and object generic models were trained for each subject. For the second part, the collected data was categorized into different groups, namely, females, males, participants with small hand size, participants with medium hand size and participants with large hand size and both RF based object specific and object generic models were trained. The decoding accuracy for subject and object specific models was as high as 83.61% (see Table II), where as for subject specific object generic models it is 73.82% (see Table III) and for the generic decoding models it is 67.58% (see Table V). Thus, it can be concluded that the more specific the decoding model is, the better is the decoding accuracy. It was also shown that for subject generic models, better accuracy can be achieved if the models are trained for subjects grouped by their hand length.

From the results, it was observed that the size of the hand affects the way someone uses her/his muscles in dexterous manipulation tasks. According to [12], the reason for this observation can be attributed to the significant variations in hand sizes, kinematics, and musculotendon sizes across different subjects. Due to such differences, the participants with smaller hand size had significantly higher importance of the opponens pollicis muscles while participants with bigger hand size had comparative importance for all muscles. It was also observed that the extensor digitorum and flexor digitorum have higher contributions for the off-center mass cube as compared to the Rubik's cube. A motion decoding model can also be generalized across different subjects, objects, and in-hand manipulation motions. Such generalized models

need to account for motion variations that may arise due to variations in hand sizes and skin thicknesses across different subjects [12]–[14], [48].

Based on the results, it can be concluded that it is feasible to develop EMG based HMI interfaces for able-bodied subjects that will be able to efficiently decode the object motion during the execution of dexterous, in-hand manipulation tasks. Such interfaces can be used in teleoperating robot arm-hand systems, developing muscle computer interfaces for games and entertainment, rehabilitation etc. This study suggests that the intrinsic muscles of the hand are far more important than the muscles of the forearm of the decoding of dexterous manipulation motions. Therefore, the lack of these muscles in case of a transradial amputee prohibits the efficient control of a myoelectric prosthesis in the execution of dexterous, in-hand manipulation tasks. For such a dexterous control of the prosthesis, shared control schemes should be developed that combine EMG based control schemes with external sensors and sophisticated control algorithms that result to semi-autonomous operation paradigms. These control schemes can be developed alongside a motion decoding model (which has a consistent performance), in order to improve the online dexterous myoelectric control overtime, by continuous interaction and adaptation of the user with the controller, as discussed in [49].

REFERENCES

[1] P. Artemiadis, "EMG-based robot control interfaces: Past, present and future," *Adv. Robot. Automat.*, vol. 1, no. 2, p. e107, 2012.

[2] J. Vogel, C. Castellini, and P. van der Smagt, "EMG-based teleoperation and manipulation with the DLR LWR-III," in *Proc. IEEE/RSJ Int. Conf. Intell. Robots Syst.*, Sep. 2011, pp. 672–678.

[3] P. K. Artemiadis and K. J. Kyriakopoulos, "EMG-based control of a robot arm using low-dimensional embeddings," *IEEE Trans. Robot.*, vol. 26, no. 2, pp. 393–398, Apr. 2010.

[4] K. Kiguchi and Y. Hayashi, "An EMG-based control for an upper-limb power-assist exoskeleton robot," *IEEE Trans. Syst., Man, Cybern., B, Cybern.*, vol. 42, no. 4, pp. 1064–1071, Aug. 2012.

[5] L. van Dijk, C. K. van der Sluis, H. W. van Dijk, and R. M. Bongers, "Learning an EMG controlled game: Task-specific adaptations and transfer," *PLoS ONE*, vol. 11, no. 8, 2016, Art. no. e0160817.

[6] T. S. Saponas, D. S. Tan, D. Morris, J. Turner, and J. A. Landay, "Making muscle-computer interfaces more practical," in *Proc. SIGCHI Conf. Hum. Factors Comput. Syst.*, 2010, pp. 851–854.

[7] D.-P. Yang *et al.*, "An anthropomorphic robot hand developed based on underactuated mechanism and controlled by EMG signals," *J. Bionic Eng.*, vol. 6, no. 3, pp. 255–263, 2009.

[8] M. W. Jiang, R. C. Wang, J. Z. Wang, and D. W. Jin, "A method of recognizing finger motion using wavelet transform of surface EMG signal," in *Proc. IEEE Eng. Med. Biol. 27th Annu. Conf.*, Jan. 2006, pp. 2672–2674.

[9] G. R. Naik and H. T. Nguyen, "Nonnegative matrix factorization for the identification of EMG finger movements: Evaluation using matrix analysis," *IEEE J. Biomed. Health Inform.*, vol. 19, no. 2, pp. 478–485, Mar. 2015.

[10] M. Liarokapis and A. M. Dollar, "Deriving dexterous, in-hand manipulation primitives for adaptive robot hands," in *Proc. IEEE/RSJ Int. Conf. Intell. Robots Syst. (IROS)*, Sep. 2017, pp. 1951–1958.

[11] Y. Kwon, A. Dwivedi, A. J. McDaid, and M. Liarokapis, "On muscle selection for EMG based decoding of dexterous, In-hand manipulation motions," in *Proc. 40th Annu. Int. Conf. IEEE Eng. Med. Biol. Soc. (EMBC)*, Jul. 2018, pp. 1672–1675.

[12] R. Balasubramanian and Y. Matsuoka, "Biological stiffness control strategies for the anatomically correct testbed (ACT) hand," in *Proc. IEEE Int. Conf. Robot. Automat.*, May 2008, pp. 737–742.

[13] B. Buchholz, T. J. Armstrong, and S. A. Goldstein, "Anthropometric data for describing the kinematics of the human hand," *Ergonomics*, vol. 35, no. 3, pp. 261–273, 1992.

[14] D. Nishikawa, W. Yu, H. Yokoi, and Y. Kakazu, "EMG prosthetic hand controller discriminating ten motions using real-time learning method," in *Proc. IEEE/RSJ Int. Conf. Intell. Robots Syst. Hum. Environ. Friendly Robots With High Intell. Emotional Quotients*, vol. 3, Oct. 1999, pp. 1592–1597.

[15] A. Dwivedi, Y. Kwon, A. J. McDaid, and M. Liarokapis, "EMG based decoding of object motion in dexterous, in-hand manipulation tasks," in *Proc. 7th IEEE Int. Conf. Biomed. Robot. BioMechatronics (Biorob)*, Aug. 2018, pp. 1025–1031.

[16] T. S. Saponas, D. S. Tan, D. Morris, R. Balakrishnan, J. Turner, and J. A. Landay, "Enabling always-available input with muscle-computer interfaces," in *Proc. 22nd Annu. ACM Symp. User Interface Softw. Technol.*, New York, NY, USA, 2009, pp. 167–176. doi: 10.1145/1622176.1622208.

[17] K. Kiguchi and Y. Hayashi, "Motion estimation based on EMG and EEG signals to control wearable robots," in *Proc. IEEE Int. Conf. Syst. Man Cybern.*, Oct. 2013, pp. 4213–4218.

[18] P. K. Artemiadis and K. J. Kyriakopoulos, "EMG-based teleoperation of a robot arm using low-dimensional representation," in *Proc. IEEE/RSJ Int. Conf. Intell. Robots Syst.*, Oct./Nov. 2007, pp. 489–495.

[19] A. V. Hill, "The heat of shortening and the dynamic constants of muscle," *Proc. R. Soc. Lond. B, Biol. Sci.*, vol. 126, no. 843, pp. 136–195, 1938.

[20] M. V. Liarokapis, P. K. Artemiadis, P. T. Katsiaris, and K. J. Kyriakopoulos, "Learning task-specific models for reach to grasp movements: Towards EMG-based teleoperation of robotic arm-hand systems," in *Proc. 4th IEEE RAS EMBS Int. Conf. Biomed. Robot. Biomechatronics (BioRob)*, Jun. 2012, pp. 1287–1292.

[21] A. Gijsberts *et al.*, "Stable myoelectric control of a hand prosthesis using non-linear incremental learning," *Frontiers Neurorobot.*, vol. 8, p. 8, Feb. 2014.

[22] N. Nazmi, M. A. Rahman, S.-I. Yamamoto, S. Ahmad, H. Zamzuri, and S. Mazlan, "A review of classification techniques of EMG signals during isotonic and isometric contractions," *Sensors*, vol. 16, no. 8, p. 1304, 2016.

[23] A. Balbinot and G. Favieiro, "A neuro-fuzzy system for characterization of arm movements," *Sensors*, vol. 13, no. 2, pp. 2613–2630, 2013.

[24] P. Zhou, B. Lock, and T. A. Kuiken, "Real time ECG artifact removal for myoelectric prosthesis control," *Physiol. Meas.*, vol. 28, no. 4, pp. 397–413, 2007.

[25] K. Englehart and B. Hudgins, "A robust, real-time control scheme for multifunction myoelectric control," *IEEE Trans. Biomed. Eng.*, vol. 50, no. 7, pp. 848–854, Jul. 2003.

[26] D. Farina and R. Merletti, "Comparison of algorithms for estimation of EMG variables during voluntary isometric contractions," *J. Electromyography Kinesiol.*, vol. 10, no. 5, pp. 337–349, 2000.

[27] A. Phinyomark, F. Quaine, S. Charbonnier, C. Serviere, F. Tarpin-Bernard, and Y. Laurillau, "EMG feature evaluation for improving myoelectric pattern recognition robustness," *Expert Syst. Appl.*, vol. 40, no. 12, pp. 4832–4840, 2013.

[28] K. Englehart, B. Hudgins, and P. A. Parker, "A wavelet-based continuous classification scheme for multifunction myoelectric control," *IEEE Trans. Biomed. Eng.*, vol. 48, no. 3, pp. 302–311, Mar. 2001.

[29] M. A. Oskoei and H. Hu, "Myoelectric control systems—A survey," *Biomed. Signal Process. Control*, vol. 2, no. 4, pp. 275–294, 2007.

[30] B. Hudgins, P. Parker, and R. N. Scott, "A new strategy for multifunction myoelectric control," *IEEE Trans. Biomed. Eng.*, vol. 40, no. 1, pp. 82–94, Jan. 1993.

[31] G. Hägg, "Electromyographic fatigue analysis based on the number of zero crossings," *Eur. J. Physiol.*, vol. 391, no. 1, pp. 78–80, Jul. 1981.

[32] C. Kendell, E. D. Lemaire, Y. Losier, A. Wilson, A. Chan, and B. Hudgins, "A novel approach to surface electromyography: An exploratory study of electrode-pair selection based on signal characteristics," *J. Neuroeng. Rehabil.*, vol. 9, p. 24, Apr. 2012.

[33] U. O. Guelph. *EMG Signals*. Accessed: Aug. 30, 2019. [Online]. Available: http://www.soe.uoguelph.ca/webfiles/mleuniss/Biomechanics/EMG.html

[34] F. E. Zajac, "Muscle and tendon Properties models scaling and application to biomechanics and motor," *Crit. Rev. Biomed. Eng.*, vol. 17, no. 4, pp. 359–411, 1989.

[35] O. Fukuda, T. Tsuji, M. Kaneko, and A. Otsuka, "A human-assisting manipulator teleoperated by EMG signals and arm motions," *IEEE Trans. Robot. Autom.*, vol. 19, no. 2, pp. 210–222, Apr. 2003.

[36] C. Castellini, P. van der Smagt, G. Sandini, and G. Hirzinger, "Surface EMG for force control of mechanical hands," in *Proc. IEEE Int. Conf. Robot. Automat.*, May 2008, pp. 725–730.

[37] A. A. Adewuyi, L. J. Hargrove, and T. A. Kuiken, "An analysis of intrinsic and extrinsic hand muscle EMG for improved pattern recognition control," *IEEE Trans. Neural Syst. Rehabil. Eng.*, vol. 24, no. 4, pp. 485–494, Apr. 2016.

[38] M. V. Liarokapis, P. K. Artemiadis, P. T. Katsiaris, K. J. Kyriakopoulos, and E. S. Manolakos, "Learning human reach-to-grasp strategies: Towards EMG-based control of robotic arm-hand systems," in *Proc. IEEE Int. Conf. Robot. Automat.*, May 2012, pp. 2287–2292.

[39] M. V. Liarokapis, P. K. Artemiadis, K. J. Kyriakopoulos, and E. S. Manolakos, "A learning scheme for reach to grasp movements: On EMG-based interfaces using task specific motion decoding models," *IEEE J. Biomed. Health Inform.*, vol. 17, no. 5, pp. 915–921, Sep. 2013.

[40] B. Calli, A. Walsman, A. Singh, S. Srinivasa, P. Abbeel, and A. M. Dollar, "Benchmarking in manipulation research: Using the yale-CMU-Berkeley object and model set," *IEEE Robot. Autom. Mag.*, vol. 22, no. 3, pp. 36–52, Sep. 2015.

[41] Z.-M. Li, V. M. Zatsiorsky, and M. L. Latash, "The effect of finger extensor mechanism on the flexor force during isometric tasks," *J. BioMech.*, vol. 34, no. 8, pp. 1097–1102, 2001.

[42] J. N. A. L. Leijnse and J. J. Kalker, "A two-dimensional kinematic model of the lumbrical in the human finger," *J. BioMech.*, vol. 28, no. 3, pp. 237–249, 1995.

[43] *Muscles of the Arm Hand—Anatomy Pictures Information*. Accessed: Aug. 30, 2019. [Online]. Available: http://www.innerbody.com/anatomy/muscular/arm-hand

[44] D. Tkach, H. Huang, and T. A. Kuiken, "Study of stability of time-domain features for electromyographic pattern recognition," *J. Neuroeng. Rehabil.*, vol. 7, no. 1, p. 21, May 2010.

[45] T. K. Ho, "Random decision forests," in *Proc. 3rd Int. Conf. Document Anal. Recognit.*, vol. 1, Aug. 1995, pp. 278–282.

[46] E. M. Kleinberg, "Stochastic discrimination," *Ann. Math. Artif. Intell.*, vol. 1, pp. 207–239, Sep. 1990.

[47] L. Breiman, "Random forests," *Mach. Learn.*, vol. 45, no. 1, pp. 5–32, 2001.

[48] C. Escoffier *et al.*, "Age-related mechanical properties of human skin: An *in vivo* study," *J. Investigative Dermatol.*, vol. 93, no. 3, pp. 353–357, 1989.

[49] N. Jiang, I. Vujaklija, H. Rehbaum, B. Graimann, and D. Farina, "Is accurate mapping of EMG signals on kinematics needed for precise online myoelectric control?" *IEEE Trans. Neural Syst. Rehabil. Eng.*, vol. 22, no. 3, pp. 549–558, May 2014.